



This is a repository copy of *Robust real-time substructuring techniques for under-damped systems*.

White Rose Research Online URL for this paper:
<http://eprints.whiterose.ac.uk/79699/>

Version: Submitted Version

Article:

Gawthrop, P.J., Neild, S.A., Wallace, M.I. et al. (1 more author) (2007) Robust real-time substructuring techniques for under-damped systems. *Structural Control and Health Monitoring*, 14. 591 - 608. ISSN 1545-2255

<https://doi.org/10.1002/stc.174>

Reuse

Unless indicated otherwise, fulltext items are protected by copyright with all rights reserved. The copyright exception in section 29 of the Copyright, Designs and Patents Act 1988 allows the making of a single copy solely for the purpose of non-commercial research or private study within the limits of fair dealing. The publisher or other rights-holder may allow further reproduction and re-use of this version - refer to the White Rose Research Online record for this item. Where records identify the publisher as the copyright holder, users can verify any specific terms of use on the publisher's website.

Takedown

If you consider content in White Rose Research Online to be in breach of UK law, please notify us by emailing eprints@whiterose.ac.uk including the URL of the record and the reason for the withdrawal request.



eprints@whiterose.ac.uk
<https://eprints.whiterose.ac.uk/>

Robust real-time substructuring techniques for under-damped systems

P. J. Gawthrop^{1,*}, M. I. Wallace², S. A. Neild², and D. J. Wagg²

¹ *Centre for Systems and Control and Department of Mechanical Engineering, University of Glasgow, GLASGOW. G12 8QQ*

UK

² *Department of Mechanical Engineering, Queens Building, University of Bristol, Bristol BS8 1TR, UK.*

SUMMARY

This paper considers the hybrid simulation of under-damped dynamical systems using numerical-experimental real-time substructuring. Substructuring joins together a physical plant with a numerical model using real time control techniques, such that the combined model emulates the behaviour of the entire system. Due to the low damping, the control of substructured systems can be highly sensitive to delay and uncertainty. We present a technique for calculating the critical delay of the substructured system using a phase margin approach. In addition, it is shown that robustness techniques, drawn from feedback control theory, can be used to reduce the destabilizing effect of uncertainty. To demonstrate this a comparison of three different robustness compensators is presented, using a well known linear system. The level of uncertainty is deliberately increased to compare their performances and a discussion is made on when each may be most useful. Copyright © 2005 John Wiley & Sons, Ltd.

KEY WORDS: Hybrid testing, substructuring, stability, robust control

*Correspondence to: P. J. Gawthrop, Centre for Systems and Control and Department of Mechanical Engineering, University of Glasgow, GLASGOW. G12 8QQ UK. P.Gawthrop@eng.gla.ac.uk

1. Introduction

In this paper we consider the recently developed structural testing method of *real-time dynamic substructuring*. This is a form of hybrid numerical-experimental testing suited to testing large structures or complex systems containing a *critical component* of interest [13]. The technique allows the critical component to be tested experimentally at full scale while the remainder of the system is modelled numerically. The coupling between the physical and numerical parts is achieved using real-time control of actuators connected to the physical substructure [1, 2, 6, 9].

As pointed out previously [4, 10], substructuring can be viewed as a control problem. However, unlike conventional control system design which aims for a well-damped closed-loop system, the corresponding substructuring design often has lightly-damped behaviour near the boundary of stability. For this reason, *robustness* is an essential consideration for this type of testing. However, because the testing technique has been developed primarily from a civil engineering perspective, robustness has not been studied using a control theoretic approach. In this paper we apply tools from control theory to study the robust stability of a generic linear substructuring system. In particular we focus on the effect of unmodelled delays and other uncertainties which occur during substructuring. We present a technique for calculating the critical delay, τ_c , beyond which the substructured system will become unstable, characterized by the onset of oscillations with positive exponential growth. Another approach for identifying this critical delay is presented by Wallace et al. [11] which uses Delay Differential Equation (DDE) models to analyse the substructured system; the relation between the two approaches is discussed in this paper.

A number of substructuring control strategies have been reported [1, 2, 4, 6, 7, 8, 9, 10, 11,

12]. These strategies consist of compensating for the combined dynamics of the actuator(s) and corresponding proprietary (i.e. built in) controller(s) — together these are referred to as the *transfer system(s)*. An additional compensator (or *outer-loop controller*) is introduced around the transfer system to eliminate the effect of its own dynamics from the force fed back from the substructure. The outer-loop controllers suggested to date broadly fall into two categories, those that provide (time) delay (e^{-sT}) compensation and those that provide lag (e.g. $\frac{1}{1+sT}$) compensation; section 2 presents more detail on these outer-loop strategies.

In this paper, the problem of robustness is considered for a generic substructuring model. In particular, robustness is a particular concern when the structure being tested is lightly damped or there is a high level of uncertainty in the transfer system control. Here we examine the stability and robustness of a substructuring algorithm and describe a strategy for increasing the control robustness for lightly-damped systems through the use of a robust transfer system design methodology. Three types of robustness compensators are proposed to address uncertainties in the transfer system model. The trade off is that control performance (in terms of accuracy of the hybrid simulation) is reduced for increased control robustness. The effects of the robustness compensators are illustrated using a single degree-of-freedom example, with both hybrid numerical-experimental results compared to pure numerical simulations, by intentionally increasing the uncertainty in the system.

2. The substructuring algorithm

To carry out a substructuring test, the numerical model and the physical substructure are run in parallel and interact in real-time to emulate the dynamic behaviour of the complete structure. This interaction is achieved through the exchange of information at the interface between the numerical model and the substructure. Firstly, the displacements (or higher state derivative) at the interface are calculated

using a numerical model and imposed via actuation devices (the transfer systems) on the physical substructure. Secondly, the forces due to imposing these displacements on the physical substructures are measured and fed back to the numerical model where they are included at the interface for the next time step. A controller is used to minimize the effects of the dynamics introduced by the transfer system. Most dynamic test methods use a proprietary controller, which typically performs PID control, to reduce the uncertainty of the transfer system dynamics to an acceptable level. However, to achieve a stable substructuring algorithm a more sophisticated compensation scheme is also required to reduce the delay introduced by the transfer system to a level below the critical limit.

The first time delay compensators were obtained by assuming that the dynamics of the transfer system may be approximated to a pure delay. For example, Horiuchi et al. [6] and Blakeborough et al. [1] proposed outer-loop forward prediction methods which use polynomial extrapolation to predict forward the numerical model displacement by a fixed number of time-steps. Darby et al. [2] relaxed the assumption of a pure delay by developing a forward prediction method that varied the amount of delay compensation, based on the error between the actuator displacement and the desired numerical model displacement. This method was extended by Wallace et al. [12] who developed an adaptive forward prediction algorithm that used variable polynomial coefficients such that non-integer multiples of the previous time step could be predicted and also incorporates an amplitude correction algorithm. The use of a Smith predictor has also been proposed as a suitable delay compensator [9].

Lag compensation via an experimental transfer function estimation of the combined inner-loop controller and actuator dynamics has been proposed by Gawthrop et al. [4] and Reinhorn et al. [9]. The proposed outer-loop controllers compensate for unwanted dynamics by applying the inverse of the transfer function estimation. Model reference adaptive control has also been suggested as an outer-loop strategy by Wagg and Stoten [10], Neild et al. [8] and Lim et al. [7] which demonstrated how lag

compensation can be achieved via this approach.

Noting that both e^{-sT} and $\frac{1}{1+sT}$ have the same first-order Taylor expansion $(1 - sT)$ – which indeed they share with more complicated transfer functions such as $\frac{1}{(1+s\frac{T}{2})^2}$ and $\frac{(1-s\frac{T}{2})}{1+s\frac{T}{2}}$ – there is not much practical difference between the approaches when the damping is small as low order approximations apply in this case. This point is examined further in Section 3.1.

[Figure 1 about here.]

Figure 1 shows two block diagram representations of substructuring[†]. Figure 1(a) shows the ideal case where a numerical substructure, **num**, is coupled directly to a physical substructure, **phy**, and there are no transfer system dynamics and hence no need for a controller. The detail of the two substructure blocks is: for **phy** the output F_p and input d_p are a collocated force and displacement pair connecting **phy** to the numerical part of the substructured system. Similarly for **num** the output F_N and input d_N are the collocated force and displacement pair connecting **num** to the physical part of the substructured system. The signal r represents the net effect of external forces in the numerical part of the model.

In this ideal situation, $F_N = F_p$ and $d_p = d_N$ and the dynamic behaviour of the substructured system exactly replicated that of the emulated system[‡]. However, for structural or mechanical systems, the physical system input d_p has to be generated by a transfer system which has the control objective of setting $d_p \approx d_N$. The physical force F_p is measured by a *sensor system* which also has its own dynamics. In practice the ideal sensor system has the relationship that $F_p \rightarrow F_N$ as $d_p \rightarrow d_N$.

Figure 1(b) gives a block diagram representation of the practical case. In addition to the two blocks of Figure 1(a); **tra** represents the controlled transfer system including both inner- and outer-loop control

[†]An alternative bond graph representation is given by Gawthrop et al. [4].

[‡]This is the case in Hardware-in-the-loop testing, where because of the structure of the system being tested, the transfer systems have no dynamics.

systems, and **mea** represents the measurement sensor system, which includes the force transducer and associated power supplies (this is assumed not to interact with **phy**). We note that physical part of **tra** usually consists of the actuator and inner-loop controller and is affected by F_P (an actuator only has a finite performance capacity envelope in which it will operate in a linear fashion), while the numerical (augmented) part of **tra** is the outer-loop controller and robustness compensator with its accuracy being affected by the measured version of F_P (F_N). At this point, the following assumption is made

Assumption 1. *The four systems in Figure 1(b) are linear, time-invariant and stable.*

Using Assumption 1, the ideal substructuring case, Figure 1(a), may be represented by:

$$F_P = P(s)d_P \quad (\mathbf{phy}), \quad (1)$$

$$d_N = N_1(s)r - N_2(s)F_N \quad (2)$$

$$= N(s)(N_r(s)r - F_N) \quad (\mathbf{num}), \quad (3)$$

where, $P(s)$ is the transfer function corresponding to **phy**, $N_1(s)$ and $N_2(s)$ in Equation (2) are separate parts of the numerical model, which we re-express in Equation (3) in a more convenient form for later analysis; $N(s)$ is the transfer function corresponding to **num** and $N_r(s)$ is a transfer function representing the interface between **num** and the external forcing. In the ideal case there are no transfer system or measurement dynamics, such that $F_N = F_P$ and $d_P = d_N$. Then Equations (1) and (3) for the physical substructure and the numerical model dynamics may be simplified such that the overall system dynamics are identical to that of the emulated system. This leads to the relation

$$F_P = \frac{L_0(s)}{1 + L_0(s)} N_r(s)r, \quad (4)$$

where $L_0(s) = P(s)N(s)$ and is defined as the *nominal* loop gain.

For the realistic substructuring representation, Figure 1(b), the dynamics of the transfer system and

the measurement system must be included. We define these dynamics as

$$d_P = T(s)d_N - T_P(s)F_P \quad (\mathbf{tra}), \quad (5)$$

$$F_N = M(s)F_P \quad (\mathbf{mea}), \quad (6)$$

where the term $T_P(s)F_P$ of Equation (5) includes the *net* effect of F_P and F_N on \mathbf{tra} . From Assumption 1, each transfer function explicitly appearing in Equations (1)–(6) is *stable*. The issue is then to investigate whether the dynamics of the substructured system shown in Figure 1(b) is also stable.

Rearranging equations (1), (3), (5) and (6) the representation of Figure 1(b) may be written as

$$[1 + P(s)T_P(s)]F_P = L_0(s)[T(s)N_r(s)r - T(s)M(s)F_P]. \quad (7)$$

Defining the *neglected* gain as $\Lambda(s)$ and the *neglected* forward gain as $\Lambda_r(s)$ we obtain

$$\Lambda(s) = [1 + P(s)T_P(s)]^{-1} T(s)M(s), \quad (8)$$

$$\Lambda_r(s) = [1 + P(s)T_P(s)]^{-1} T(s). \quad (9)$$

Defining an *equivalent* force, $F_e = \Lambda_r(s)N_r(s)r$, the system dynamics may be expressed as

$$F_P = L_0(s)[F_e - \Lambda(s)F_P]. \quad (10)$$

Figure 1(b) can thus be represented by the classical feedback system of Figure 2.

[Figure 2 about here.]

Finally, defining $D(s)$ as the transfer function relating F_e and F_P for the practical substructured system, using (10) we can write:

$$D(s) = \frac{L_0(s)}{1 + \Lambda(s)L_0(s)}, \quad (11)$$

such that

$$F_P = D(s)F_e. \quad (12)$$

Using Equation (4) and recognising that for the ideal case $\Lambda(s) = \Lambda_r(s) = 1$, the corresponding nominal transfer function relating to the ideal substructured system, and the emulated system, may be defined as

$$D_0(s) = \frac{L_0(s)}{1 + L_0(s)}. \quad (13)$$

In Section 4 we discuss the use of different robustness compensation schemes. We note that $D_0(s)$ will explicitly include these algorithms and therefore change. Thus for comparison, we define D_{em} as the emulated system transfer function such that $D_{em} = D_0(s)$ when $L_0(s)$ does not incorporate any compensation schemes.

3. Relative and robust stability

Figure 2 and the corresponding closed-loop system (12) are in the classical feedback control system form where $L_0(s)$ would be interpreted as the “system” and $\Lambda(s)$ as the “controller”. This means that a range of standard control system design techniques (Goodwin et al. [5] gives a comprehensive exposition) can be brought to bear on the problem.

For example, *relative stability* [5, sec. 5.8] can be characterized as follows. Define the *critical frequency* ω_c as the solution of

$$|L(j\omega_c)| = 1, \quad (14)$$

where the *actual* loop gain, $L(s)$, is defined as

$$L(s) = \Lambda(s)L_0(s). \quad (15)$$

The corresponding *phase margin* ϕ_m may be written as

$$\phi_m = \pi - \angle L(j\omega_c). \quad (16)$$

The phase margin provides a measure of how near to instability the ideal system (where $\Lambda(s) = 1$) is in terms of how much phase lag (due to $\Lambda(s) \neq 1$) is permissible. For example, if the neglected dynamics comprise a pure delay ($\Lambda(s) = e^{-s\tau}$) then the *critical delay*, τ_c , is the time delay which would give a phase lag of ϕ_m and is given by

$$\tau_c = \frac{\phi_m}{\omega_c}. \quad (17)$$

This gives an alternative method for computing the critical delay, in addition to that developed by Wallace et al. [11] which uses Delay Differential Equation (DDE) models. For the class of system for which the DDE methods cannot be applied or when it is impractical to use the technique, Equation (17) could still be used in many cases (even if only as a linear approximation) to give an estimate of τ_c . The link between the two techniques is discussed further in Section 3.1.

For substructuring systems in the form developed in Section 2 we would like to apply more general, *robust stability* methods. Using the approach outlined in [5, sec. 5.9], together with the assumption that both $L_0(s)$ and $\Lambda(s)$ are stable implies that the closed-loop system of Figure 2 is stable if

$$|D_0(j\omega)| |\Delta(j\omega)| \leq 1 \quad \forall \omega, \quad (18)$$

where

$$\Delta(s) = \Lambda(s) - 1. \quad (19)$$

This is a conservative result but has the advantage of bounding the error transfer function Δ in terms of the desired system $D_0(j\omega)$. In particular it shows that $\Delta(j\omega)$ must be small at those frequencies where $D_0(j\omega)$ is large — typically at the resonant frequencies of the desired system.

Although these methods are standard in the control system context, they are novel in the substructuring context. In particular, both relative and robust stability can be reinterpreted for substructuring; a motivational example appears in Section 3.1.

3.1. Substructuring Example

[Figure 3 about here.]

[Figure 4 about here.]

[Figure 5 about here.]

An example of a substructured system is shown schematically in Figure 3. The system has a numerical substructure consisting of a mass of m kg, a spring with stiffness k N/m and damper with constant c Ns/m and a physical substructure consisting of a spring with stiffness k_s N/m. This corresponds to the hybrid numerical-experimental system which will be presented in Section 5. In this case

$$L_0(s) = \frac{k_s}{ms^2 + cs + k}, \quad (20)$$

$$N_r(s) = cs + k. \quad (21)$$

Defining the natural frequency of the numerical subsystem as $\omega_n = \sqrt{\frac{k}{m}}$, the corresponding damping ratio $\zeta = \frac{c}{2m\omega_n}$ and $p = \frac{k_s}{k}$ we can write

$$L_0(s) = \frac{p\omega_n^2}{s^2 + 2\zeta\omega_n s + \omega_n^2}, \quad (22)$$

$$N_r(s) = m(2\zeta\omega_n s + \omega_n^2). \quad (23)$$

Defining $\hat{s} = \frac{s}{\omega_n}$, this can be rewritten in normalised form as

$$L_0(s) = \frac{p}{\hat{s}^2 + 2\zeta\hat{s} + 1}, \quad (24)$$

$$N_r(s) = k(2\zeta\hat{s} + 1). \quad (25)$$

Defining $\hat{\omega} = \frac{\omega}{\omega_n}$ and using (14), the critical frequency corresponding to (24) is the solution of

$$(1 - \hat{\omega}^2)^2 + 2\zeta^2\hat{\omega}^2 - p^2 = \hat{\omega}^4 + (4\zeta^2 - 2)\hat{\omega}^2 + (1 - p^2) = 0. \quad (26)$$

Equation (26) is quadratic in $\hat{\omega}^2$. It has real solutions if

$$(4\zeta^2 - 2)^2 > (1 - p^2). \quad (27)$$

There are two cases: if $p \geq 1$ then Equation (27) is independent of ζ , otherwise the condition depends on the value of ζ . In the case of real solutions, the positive square root of a positive solution gives a (positive) value of $\hat{\omega}$ satisfying Equation (14).

Figure 4(a) shows $\log |L_0(j\hat{\omega})|$ plotted against $j\hat{\omega}$ for $p = 1$ and $\zeta = 0.107$. In this case, $\hat{\omega}_c = 1.398$, the frequency at which $|L_0(j\hat{\omega})| = 1$. Figure 4(b) gives the corresponding phase (in degrees) indicating a phase margin of $17.34^\circ = 0.3027\text{rad}$. This gives a critical delay of $\hat{\tau}_c = 0.2165$, which is precisely the value obtained from the DDE numerical analysis of Wallace et al. [11] confirming the fact that both methods are exact. However, the method of this paper gives a different insight into the problem and has a number of advantages: it can be used for more complicated examples than can the DDE approach and is applicable to uncertainties modelled by *any* transfer function.

The corresponding diagrams for $L = e^{-j\hat{\omega}}L_o$ are plotted in Figures 4(a) and 4(b). As predicted, $L(j\hat{\omega}_c) = -1$ corresponding to $|L(j\hat{\omega}_c)| = 1$ and $\angle L(j\hat{\omega}_c) = -180^\circ$.

Figure 5(a) shows how the phase margin varies with ζ and 5(b) how it varies with p . For small values of ζ , the phase margin ϕ_m is approximately proportional to ζ . Larger values of p give a reduced phase margin. Figure 4(a) also provides alternative insight into the solution of Equation (26). From Equation (24), the sole effect of p is to move the curve of Figure 4(a) vertically. It is therefore clear that when $p > 1$, $\log |L_0(j\hat{\omega})| = 0$ at only one frequency implying a single positive real solution of Equation (26) for $\hat{\omega}^2$. On the other hand, if $p < 1$ there is no solution if the peak of the curve is below zero. From Equation (24), the peak value occurs at an approximate frequency of $\hat{\omega} = 1$ where $|L_0(j\hat{\omega})| = \frac{p}{2\zeta}$. Thus, as also indicated in Figure 5(b), the phase margin is infinite when $p < 2\zeta$.

[Figure 6 about here.]

The robustness criterion Equation (18) can be examined by plotting both $\frac{1}{|D(j\omega)|}$ and $|\Delta(j\omega)|$ on the same diagram. For example, Figure 6(a) shows $\frac{1}{|D(j\omega)|}$ when $p = 1$ and $\zeta = 0.107$. On the same diagram, $|\Delta(j\omega)|$ is plotted for two cases:

$$\Lambda(\hat{s}) = \begin{cases} e^{-\hat{\tau}\hat{s}}, & \text{(shown as } \Delta_d \text{ in Figure 6(a))} \\ \frac{1}{1+\hat{\tau}\hat{s}}, & \text{(shown as } \Delta_l \text{ in Figure 6(a))} \end{cases} \quad (28)$$

where $\hat{\tau} = 0.21$. In this case, stability is predicted in each case as Equation (18) is satisfied. However, this would not be the case if τ were increased slightly. Note that both forms of $\Lambda(\hat{s})$ of Equation (28) give similar results in this case indicating that *phase* error is more important than *amplitude* error in this case. Note that $\hat{\tau} = 0.21$ predicted by this (conservative) robust stability method is less than that predicted by the exact relative stability (phase margin) approach. However, the robustness approach is more general in that the uncertainty does not need to be parameterized by a transfer function.

The minimum value of $\frac{1}{|D(j\omega)|}$ occurs at $\hat{\omega}^2 \approx (1+p)$ with a value of approximately $\frac{2\zeta\sqrt{1+p}}{p}$. Noting that the maximum value of $\Delta = 1 - e^{-\hat{\tau}\hat{s}}$ is 2, it follows that the substructured system will be stable for *any* delay τ if

$$\zeta > \frac{p}{\sqrt{1+p}}. \quad (29)$$

Figure 6(b) shows the boundary implied by Equation (29).

4. A Robust Transfer System Design Methodology

This paper provides a stability and robustness *analysis* of the substructuring problem by applying techniques from linear control theory. This leads on to a methodology for the *design* of the transfer system to achieve robust stability. The use of linear theory — and particularly the assumptions that the experimental substructure and transfer systems are approximated by linear transfer functions — would

at first sight appear to be a serious limitation of this analysis. However, these results can be applied to — and in some cases can significantly improve results from — substructuring tests with nonlinear elements. This is because a robust linear system can cope with a significant amount of nonlinear ‘disturbance’. Using this approach we are able to get a good comparison of results between three different types of robustness compensator — shown in section 5.

Using linear analysis, we propose a 4 stage controller design strategy for each transfer system (which in this work we assume to be an actuator):

1. Design an (or use the proprietary) inner-loop controller around the actuator to reduce uncertainty and non-linearity in the resultant closed-loop transfer system.
2. Use system identification to estimate a (closed-loop) transfer function of the actuator and inner-loop controller (which we define as the *nominal* model). Use the same system identification results to estimate an *uncertainty* model for the transfer system.
3. Use the *nominal* model from step 2 to design an outer-loop *transfer system cancellation* controller.
4. Use the *uncertainty* model from step 2 to design a robustness compensator.

Broadly, the literature outlined in Section 2 addresses steps 1–3; the selection of the inner-loop controller gains, a system identification of the resulting transfer system and the design of an outer-loop controller to compensate for the transfer system dynamics. The adaptive nature of the outer-loop controllers proposed in [2, 8, 12] allow for the compensation of the transfer system dynamics despite uncertainty in the transfer function model derived in step 2. Although they incorporate some level of robustness due to this adaptation, they do not explicitly include the robustness compensator proposed in step 4. This is the key reason why the linear results can be applied so readily to systems where the experimental substructure is nonlinear. The adaptive nature of the outer-loop controller (in this case the

adaptive forward prediction of Wallace et al. [12]) plus the robustness compensation allows the system to cope with a significant degree of nonlinear ‘disturbance’. We note also that the analysis applies primarily to the design of the transfer system. In fact we wish to design a stable robust control strategy to eliminate (or at least mitigate) the effect of uncertainty and non-linearity from the transfer system — we want to make the transfer system dynamics linear. The only time we actually require a definition of the transfer function of the physical substructure (which is usually a nonlinear element [13]) is in order to apply the robustness compensation technique based on physical model emulation, as described in Section 4.3.

From Section 3, it is clear that instability can still occur even in the presence of apparently quite small neglected dynamics; in other words, the nominal design is not necessarily robust. However, the trade off for achieving a robust system is a reduced level of *nominal* performance.

There are three approaches suggested here

1. Damping-ratio compensation: ζ -robustness
2. Phase-advance compensation: α -robustness
3. Physical model emulation: γ -robustness

All three approaches have a single parameter which provides a trade-off between performance and robustness and are considered in the following sections. Section 4.4 gives a specific example. Methods 1 and 3 are believed to be new and have been developed specifically with substructuring in mind [4, 12]; method 2 is a standard control system technique [5, section 6.6] applied here for the first time to substructuring. Method 3 is related to the Youla parametrisation of all stabilising controllers [5, section 15.3].

4.1. Damping-ratio compensation: ζ -robustness

From Figure 6(a), it is clear that it is the magnitude of the resonant peak of the closed-loop transfer function $|D_0(j\omega_c)|$ that restricts the maximum allowed value of uncertainty $|\Lambda(j\omega_c)|$. As $|D_0(j\omega_c)|$ decreases with increasing damping, a simple way of trading robustness for stability is to increase the damping coefficients of the numerical model above their correct values.

This method has the advantage of requiring no knowledge about the system properties but has the disadvantage of distorting the nominal closed loop system.

4.2. Phase-advance compensation: α -robustness

The example of Section 3.1 implies that lack of robustness is due to the neglected phase lag associated with $\Lambda(j\omega)$ at $\omega = \omega_c$. One way to improve robustness is to deliberately introduce phase advance, at the critical frequency, to $\Lambda(j\omega)$ by interposing a phase advance transfer function between **num** and **tra**. Perhaps the simplest such transfer function is [5, sec. 6.6]:

$$C(s) = \frac{\alpha s + \omega_c}{\frac{1}{\alpha} s + \omega_c} \quad (30)$$

where the parameter $\alpha \geq 1$. Clearly $\alpha = 1$ corresponds to a unit transfer function which has no effect; the maximum phase advance occurs at about $\omega = \omega_c$. The maximum phase advance rises to about $\frac{\pi}{4}$ rad = 45° which when $\alpha \approx 10$ [5, sec. 6.6]. Typically, for this application, $1 < \alpha < 2$.

This method has the advantage of requiring only knowledge of ω_c , but has the disadvantage of distorting the nominal closed loop system.

4.3. Physical model emulation: γ -robustness

[Figure 7 about here.]

In addition to the numerical simulation of the **num** subsystem, this approach also simulates the **phy**

subsystem. As indicated in block diagram form in Figure 7(a), the output of **num** is fed into both the simulation of **phy** and the physical subsystem **phy**. In comparison to Figure 2, there are *two* feedback loops: γ times the output of the physical system and $(1 - \gamma)$ is fed back to the input of the numerical subsystem. At the two extremes, $\gamma = 0$ gives a purely numerical simulation (and $\Lambda(s)$ is not part of the feedback), whereas $\gamma = 1$ gives the hybrid numerical/physical simulation discussed in the preceding sections. When $0 \leq \gamma \leq 1$, there is a smooth transition between the two extremes. However, for each value of γ , the *nominal* closed loop system dynamics are the same.

The block diagram of Figure 7(a) can be rewritten in the simplified form of Figure 7(b) where

$$L_\gamma(s) = \frac{\gamma L_0(s)}{1 + (1 - \gamma)L_0(s)}. \quad (31)$$

The robustness results of Section 2 can then be applied to Figure 7(b) in a similar way as to that discussed for Figure 2.

This method has the disadvantage of requiring an accurate model of the physical system transfer function $P(s)$ but has the advantage of *not* distorting the nominal closed loop system.

4.4. Example (continued)

[Figure 8 about here.]

Figure 8(a) is the same as Figure 6(a) except that the results of each of the three compensators are shown as well. In each case, the stability margin is significantly increased at the resonant frequency; in each case, $\hat{\tau} \approx 0.35$, about $\frac{0.35}{0.21} = 1.67$ larger than the uncompensated case.

Figure 8(b) shows the closed loop system when the actual system (comprising the nominal system and the time delay) is compensated by the three robustness compensators. Although, as expected, these three closed-loop responses differ from the nominal (D_0) they are better than the uncompensated case which displays a large resonant peak indicating near-instability.

The other observation from Figure 8(a) is that there are significant differences between $1/|D|$ for the three different compensation methods. This will be discussed in more detail in relation to the hybrid numerical-experimental results shown in the next section.

5. Hybrid testing

[Figure 9 about here.]

The proposed robustness methods were evaluated using a small-scale substructuring experiment of the system described in Section 3.1. For the experiments, the numerical model and outer-loop compensator were written in the Matlab Simulink environment and run in real-time on a DSP using a dSpace DS1104 Controller Board. The transfer system is a linear electro-mechanical actuator attached to a centralising plate which is free to run via linear bearings on three guide rails, as shown in Figure 9. The physical substructure is a spring of stiffness $k_s = 2250\text{Nm}^{-1}$, which is held rigid at one end and attached to the actuator centralising plate via a load cell at the other.

5.1. Robust Transfer System Design

The experimental equipment has been extensively analysed and it is known that a good model for the neglected dynamics of the system under an inner-loop proportional (P) control with $k_p = 1$ is a pure delay $\Lambda(s) \approx e^{-s\hat{\tau}}$ where $\hat{\tau} \approx 0.29$. Using the parameters for this example and Equation (17) the critical value of the delay is found to be $\hat{\tau}_c \approx 0.2$. Therefore this system is *unstable* without some form of delay compensation because $\hat{\tau} > \hat{\tau}_c$. In this present study we are interested in robustness, therefore we will use the delay compensation method of Wallace et al. [12] as step 3 of the robust transfer system design methodology to make the system stable such that $\hat{\tau}$ is in the range $0 \leq \hat{\tau} < \hat{\tau}_c$. Then to highlight the effects of the three different robustness compensators, we are able to select a $\hat{\tau}$ value as appropriate

within the stable range of $0 \leq \hat{\tau} < \hat{\tau}_c$ by varying the parameters of the delay compensation scheme. This is a simple way of varying the degree of uncertainty in the system, and gives an indication of the performance of each robustness compensator as uncertainty increases.

[Table 1 about here.]

Table I summaries the values of $\hat{\tau}$ used to generate the hybrid numerical-experimental results shown in Figures 10–12. For each $\hat{\tau}$ value, Table I shows the ratio $\hat{\tau}/\hat{\tau}_c$ to give an indication of how close the system is to the stability boundary at $\hat{\tau}/\hat{\tau}_c = 1$.

5.2. Numerical-experimental results

Each of Figures 10–12 shows hybrid numerical-experimental results for four cases: no compensation, γ -compensation, ζ -compensation and α -compensation. Each plot shows three sets of data. Circles correspond to hybrid numerical-experimental measurements of $|D(j\hat{\omega})|$ (11) at six frequencies: 3.0Hz, 5.0Hz, 6.5Hz, 7.1Hz, 8.0Hz and 9.0Hz. The solid and dashed lines are the theoretical values of $|D(j\hat{\omega})|$ (with $\Lambda(\hat{s}) \approx e^{-s\hat{\tau}}$ (11) and $|D_0(j\hat{\omega})|$ (where $\Lambda(\hat{s}) = 1$) (13) respectively.

[Figure 10 about here.]

Figure 10 shows the case where $\hat{\tau} = 0$ (i.e. the delay compensation method is removing the full 9.4ms of delay in the system). In this case $|D(j\hat{\omega})|$ and $|D_0(j\hat{\omega})|$ are indistinguishable and the uncertainty is very low such that $\Lambda \approx 1$ and $|D| \approx |D_0|$. With no compensation (Figure 10 (a)) there is good agreement between the hybrid numerical-experimental results and $|D_0(j\hat{\omega})|$, indicating (as expected) that for this hybrid test setup the delay compensation method of Wallace et al. [12] provides a significant degree of robustness without an additional compensator. Figure 10 (b) shows the γ -compensation case where there is no distortion of $|D_0(j\hat{\omega})|$, and close agreement with the hybrid results. Figures 10 (c) and (d)

show the ζ -compensation and α -compensation respectively. In each case the robustness is improved — indicated by an increased phase margin — but $|D_0(j\hat{\omega})|$ is distorted. Agreement with the hybrid test results is good although the α -compensation loses some correlation near resonance.

[Figure 11 about here.]

Figure 11 shows the case where $\hat{\tau} = 0.1$. This case corresponds to the situation when the delay compensation method (step 3 in Section 4) is not fully compensating for the delay error. This can be seen in Figures 11 (a)-(d) as the discrepancy between $|D|$ and $|D_0|$ close to resonance. Now without any robustness compensation, the resonance peak $|D(j\hat{\omega})|$ becomes significantly exaggerated near the resonant frequency compared to the nominal case $|D_0(j\hat{\omega})|$. In Figures 11 (b)-(d) the three robustness compensators results are shown. The γ -compensation results give a significant improvement in reducing $|D(j\hat{\omega})|$ to $|D_0(j\hat{\omega})|$. The ζ -compensation and α -compensation also achieve the same effect, but with significant distortions in the $|D_0(j\hat{\omega})|$ transfer function. In all three compensation cases the hybrid results match well with $|D(j\hat{\omega})|$.

[Figure 12 about here.]

Figure 12 shows the case where $\hat{\tau} = 0.19$. This case corresponds to the situation when the delay compensation method is stabilising the system, but leaving a significant delay error – corresponding to a higher degree of uncertainty in the system. This can be seen clearly in Figure 12 (a) where now the discrepancy between $|D(j\hat{\omega})|$ and $|D_0(j\hat{\omega})|$ is even more pronounced close to resonance. The compensation methods shown in Figures 12 (b)–(d) all help to reduce this significantly. As with the previous example the hybrid results correlate well with $|D(j\hat{\omega})|$ across the frequency range considered.

The robustness compensation schemes can therefore be summarized by the following strengths and weaknesses:

γ -compensation has the advantage of not modifying the overall system response but is based on having an accurate model of the physical system – this was available for the experimental considered here but would not generally be available. In less well known experimental equipment, details of $\Lambda(\hat{s})$ would be unknown and thus initial experiments would use $\gamma = 1$. γ could then be decreased as more experimental results allowed reduction of the uncertainty encapsulated in $\Lambda(\hat{s})$.

ζ -compensation does not require a model of the physical system but does change the overall system characteristics; however, it has a clear physical meaning as a numerical model with an increased damping ratio.

α -compensation again does not require a model but does distort the the overall system characteristics significantly.

6. Conclusion

Hybrid testing of under-damped dynamical systems using numerical-experimental real-time substructuring is sensitive to both transfer system delay and uncertainty. The four stage robust transfer system design methodology presented in the paper is designed to reduce both of these destabilizing effects.

A phase margin approach to calculating the relative and robust critical delay is presented in Section 3, such that a cancellation controller (step 3) can be designed to ensure the stability of the substructuring algorithm when there is zero uncertainty in the nominal model of the transfer system. However, due to the characteristic nature of experimental testing, uncertainty is never negligible, especially the first time a test is performed. Therefore, it is shown in Section 4 that robustness techniques (step 4) drawn

from feedback control theory can reduce this destabilizing effect. Three methods for reducing the effect of uncertainty are discussed using theoretical and experimental results in Section 5, which show that each is effective in increasing robustness to uncertainty.

A pragmatic view of robustness is that the amount of compensation would be large for initial experiments, but would reduce as uncertainty was reduced. For example, using an advanced system identification technique as suggested by Gawthrop et al. [4] or when using an adaptive cancellation controller for step 3 of the robust transfer system design methodology. It should be noted that the lower the damping in the system the greater the destabilizing the effect both the transfer system delay and uncertainty have on the substructuring algorithm.

Noting that the linear robustness criterion (18) is closely related to the small-gain theorem and circle criterion [3] for nonlinear systems, we believe that the approach can be rigorously extended to the non-linear case.

ACKNOWLEDGEMENT

Peter Gawthrop is a Visiting Fellow at Department of Mechanical Engineering, University of Bristol.

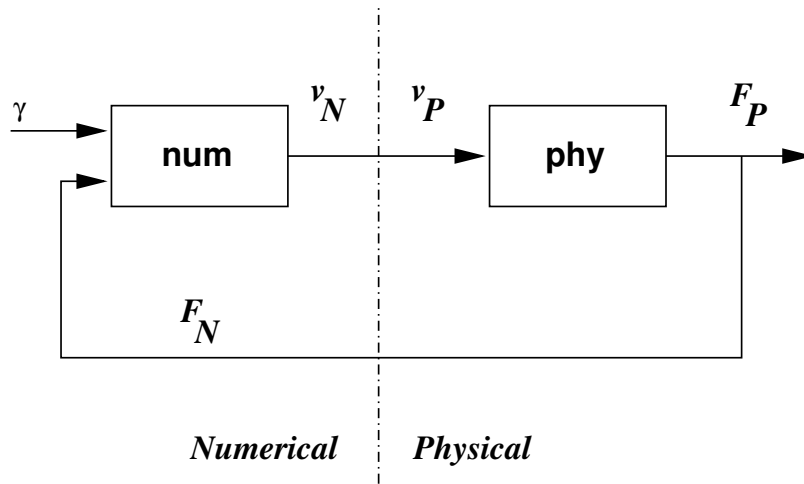
references

- [1] A. Blakeborough, M. Williams, A. Darby, and D. Williams. The development of real-time substructure testing. *Philosophical Transactions of the Royal Society pt. A*, 359(1869-1891), 2001.
- [2] A. Darby, M. Williams, and A. Blakeborough. Stability and delay compensation for real-time substructure testing. *ASCE Journal of Engineering Mechanics*, 128:1276–1284, 2002.
- [3] C. A. Desoer and M. Vidyasagar. *Feedback Systems: Input-Output Properties*. Academic Press, London, 1975.

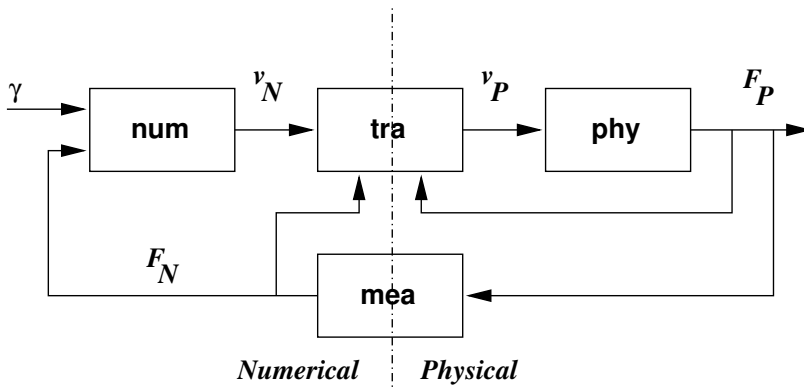
- [4] P. Gawthrop, M. Wallace, and D. Wagg. Bond-graph based substructuring of dynamical systems. *Earthquake Engng Struc. Dyn.*, 34(6):687–703, May 2005. URL <http://dx.doi.org/10.1002/eqe.450>.
- [5] G. Goodwin, S. Graebe, and M. Salgado. *Control System Design*. Prentice Hall, 2001.
- [6] T. Horiuchi, M. Inoue, T. Konno, and Y. Namita. Real-time hybrid experimental system with actuator delay compensation and its application to a piping system with energy absorber. *Earthquake Engng Struc. Dyn.*, 28:1121–1141, 1999.
- [7] C. Lim, S. Neild, D. Stoten, C. Taylor, and D. Drury. Using adaptive control for dynamic substructuring tests. In *Thirteenth World Conference on Earthquake Engineering*, Vancouver, August 2004. Paper No 2529.
- [8] S. Neild, D. Drury, and D. Stoten. An improved substructuring control strategy based on the MCS adaptive control algorithm. *Proceedings of the Institution of Mechanical Engineers Pt. I: Journal of Systems and Control Engineering*, 2005. (Accepted).
- [9] A. Reinhorn, M. Sivaselvan, Z. Liang, and X. Shao. Real-time dynamic hybrid testing of structural systems. In *Thirteenth World Conference on Earthquake Engineering*, Vancouver, August 2004. Paper No 1644.
- [10] D. Wagg and D. Stoten. Substructuring of dynamical systems via the adaptive minimal control approach. *Earthquake Engng Struc. Dyn.*, 30(6):865–877, June 2001.
- [11] M. Wallace, J. Sieber, S. Neild, D. Wagg, and B. Krauskopf. A delay differential equation approach to real-time dynamic substructuring. *Earthquake Engng Struc. Dyn.*, 2005. (Accepted).
- [12] M. Wallace, D. Wagg, and S. Neild. An adaptive polynomial based forward prediction algorithm for multi-actuator real-time dynamic substructuring. *Transactions of the Royal Society*, May 2005. (Accepted).
- [13] M. Williams and A. Blakeborough. Laboratory testing of structures under dynamic loads: an introductory review. *Philosophical Transactions of the Royal Society*, 359:1651–1669, 2001.

List of Figures

1	Substructuring: block diagram approach	23
2	Sensitivity feedback system	24
3	A substructured system.	25
4	Sensitivity: Phase margin. (a) shows the log magnitude of the nominal $\log L_0 $ and actual $\log L $ plotted against log normalised frequency $\log \hat{\omega}$; because there is only a phase error (pure delay), the curves are the same; the critical frequency $\hat{\omega}_c$ is marked by a vertical line and a unit gain by a horizontal line. (b) shows the corresponding phases together with a vertical line at the critical frequency $\hat{\omega}_c$ and a horizontal line at -180° . The phase margin is the vertical distance between -180° and the corresponding phase curve $\angle L_0(j\hat{\omega})$ at $\hat{\omega} = \hat{\omega}_c$. In this case, the actual system is such that the neglected time delay is on the boundary of stability.	26
5	Sensitivity: dependence on parameters. (a) shows how the phase margin ϕ_m depends on ζ for three values of p ; in this case, the phase margin ϕ_m <i>increases</i> with ζ . (b) shows how how the phase margin ϕ_m depends on p for three values of ζ ; in this case, the phase margin ϕ_m <i>decreases</i> with p	27
6	Robustness. (a) Shows the inverse magnitude of $D(j\hat{\omega})$ against $j\hat{\omega}$ on a logarithmic scale. For comparison two possible uncertainty transfer functions $e^{-j\hat{\omega}\hat{\tau}}$ and $\frac{1}{1+j\hat{\omega}\hat{\tau}}$ are plotted for $\hat{\tau} = 0.21$. (b) Shows the boundary of stability for <i>any</i> delay.	28
7	γ -robustness	29
8	Robustness Compensation. (a) The inverse magnitude of $D(j\hat{\omega})$ is plotted against $j\hat{\omega}$ on a logarithmic scale for the three robustness compensators with $\alpha = 1.5$, $\zeta_r = 2\zeta$ and $\gamma = 0.5$. For comparison two possible uncertainty transfer functions $e^{-j\hat{\omega}\hat{\tau}}$ and $\frac{1}{1+j\hat{\omega}\hat{\tau}}$ are plotted for $\hat{\tau} = 0.35$. (b) The lines marked α , ζ and γ give the corresponding closed-loop systems for each compensator, in the presence of $e^{-j\hat{\omega}\hat{\tau}}$. The case of no compensator, with (none) and without (D_0) delay, is given for comparison	30
9	Experimental Equipment: the linear electro-mechanical actuator is on the left of the picture and the physical substructure (spring) is on the right. Two of the three guide rails are visible crossing the picture horizontally.	31
10	Experimental Results: $\hat{\tau} = 0.00$. In this case the uncertainty is very low so $\Lambda \approx 1$ and $ D \approx D_0 $ in all four cases. γ -compensation does not distort $ D $ but ζ and α -compensation do. The experimental fit is good in each case.	32
11	Experimental Results: $\hat{\tau} = 0.10$. There is a small amount of uncertainty due to the neglected delay so $\Lambda \neq 1$ and $ D \neq D_0 $ in each case. No compensation leads to an exaggerated resonant peak which is reduced by each of the three compensators. The experimental fit is good in each case.	33
12	Experimental Results: $\hat{\tau} = 0.19$. There is a large amount of uncertainty due to the neglected delay so $\Lambda \neq 1$ and $ D \neq D_0 $ in each case. No compensation leads to an almost unstable system with almost no damping and an excessive resonant peak which far from the nominal. Each of the three compensators stabilises the system giving a peak much closer to the nominal. The experimental fit is good in each case.	34



(a) Ideal substructured model



(b) Practical substructured model

Figure 1. Substructuring: block diagram approach

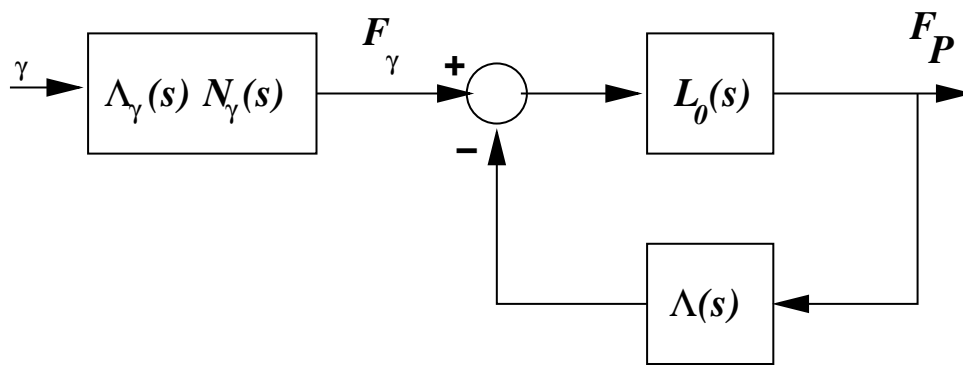


Figure 2. Sensitivity feedback system

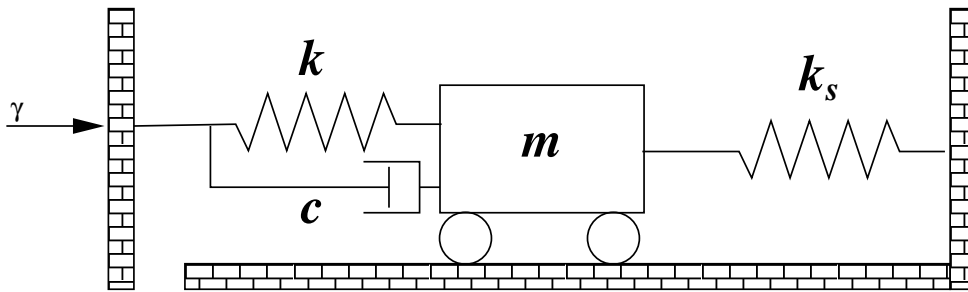


Figure 3. A substructured system.

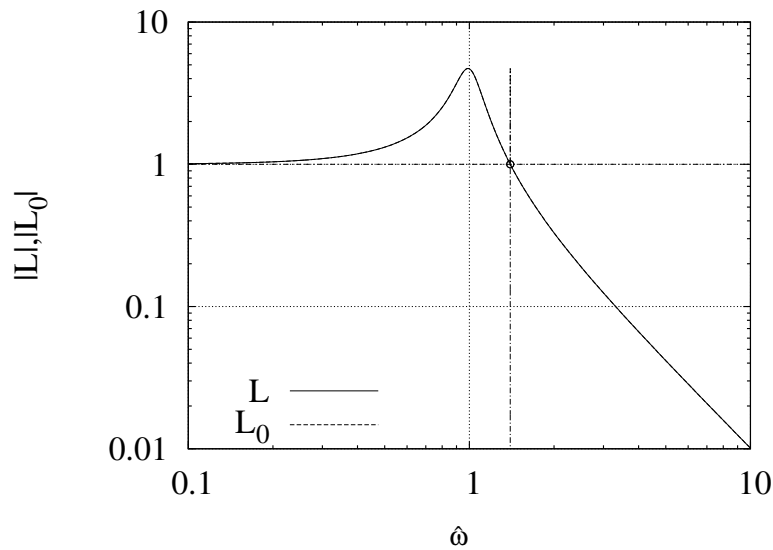
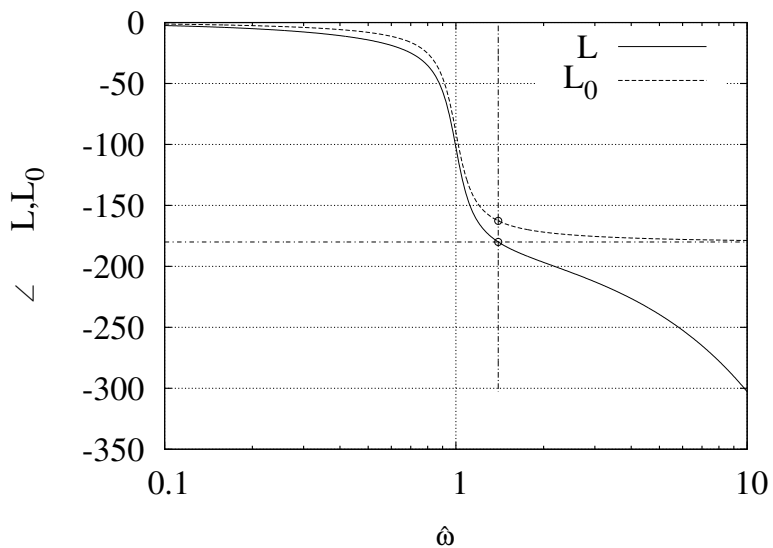
(a) $\log |L_0(j\hat{\omega})|$ & $\log |L(j\hat{\omega})|$ v. $\log \hat{\omega}$ (b) $\angle L_0(j\hat{\omega})$ & $\angle L(j\hat{\omega})$ v. $\log \hat{\omega}$

Figure 4. Sensitivity: Phase margin. (a) shows the log magnitude of the nominal $\log |L_0|$ and actual $\log |L|$ plotted against log normalised frequency $\log \hat{\omega}$; because there is only a phase error (pure delay), the curves are the same; the critical frequency $\hat{\omega}_c$ is marked by a vertical line and a unit gain by a horizontal line. (b) shows the corresponding phases together with a vertical line at the critical frequency $\hat{\omega}_c$ and a horizontal line at -180° . The phase margin is the vertical distance between -180° and the corresponding phase curve $\angle L_0(j\hat{\omega})$ at $\hat{\omega} = \hat{\omega}_c$. In this case, the actual system is such that the neglected time delay is on the boundary of stability.

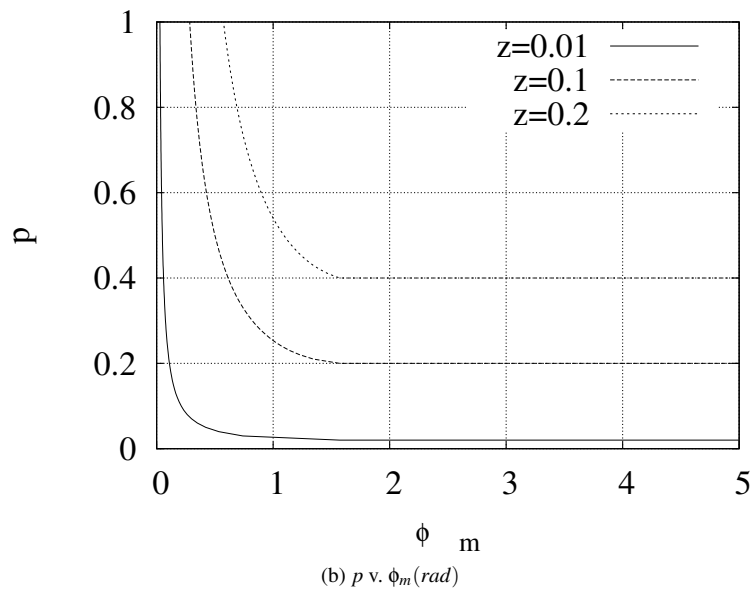
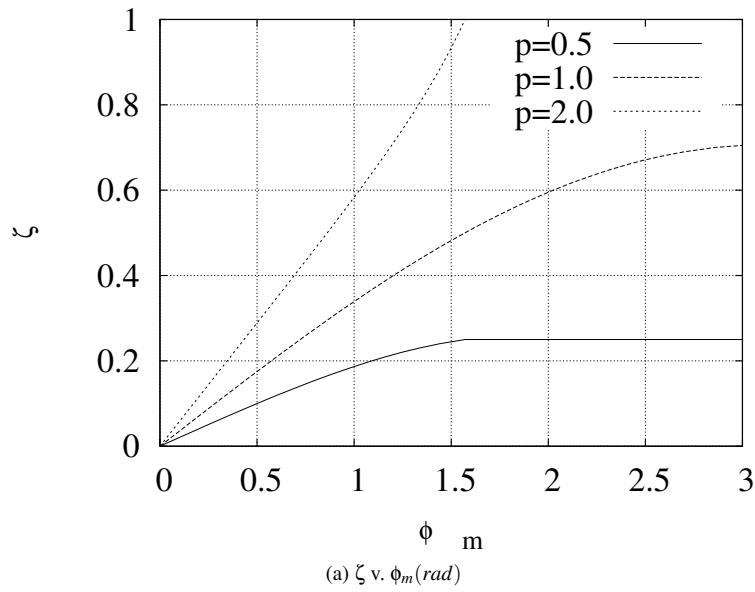
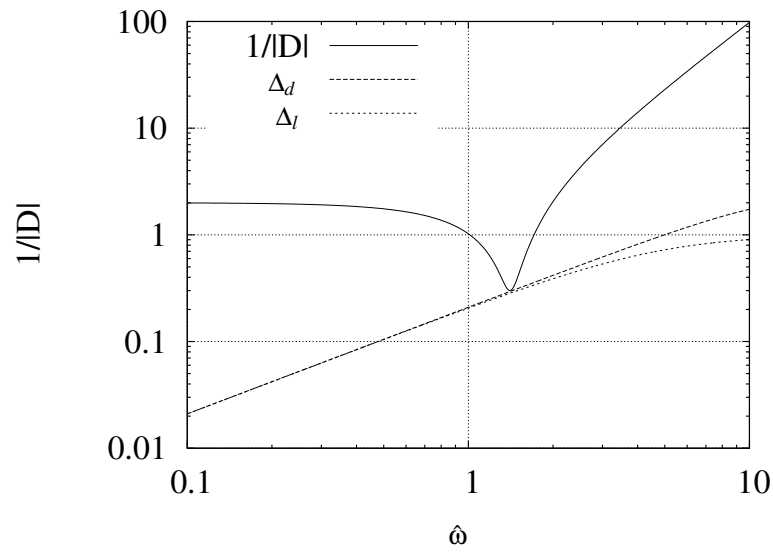
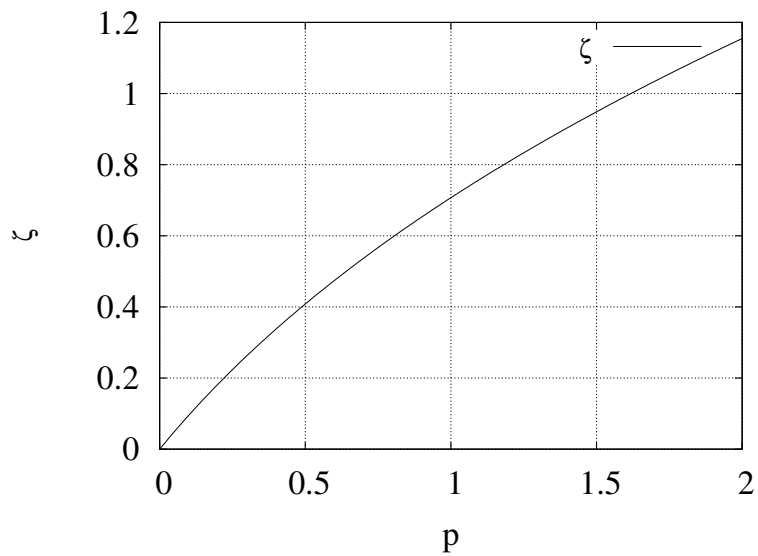


Figure 5. Sensitivity: dependence on parameters. (a) shows how the phase margin ϕ_m depends on ζ for three values of p ; in this case, the phase margin ϕ_m increases with ζ . (b) shows how the phase margin ϕ_m depends on p for three values of ζ ; in this case, the phase margin ϕ_m decreases with p .

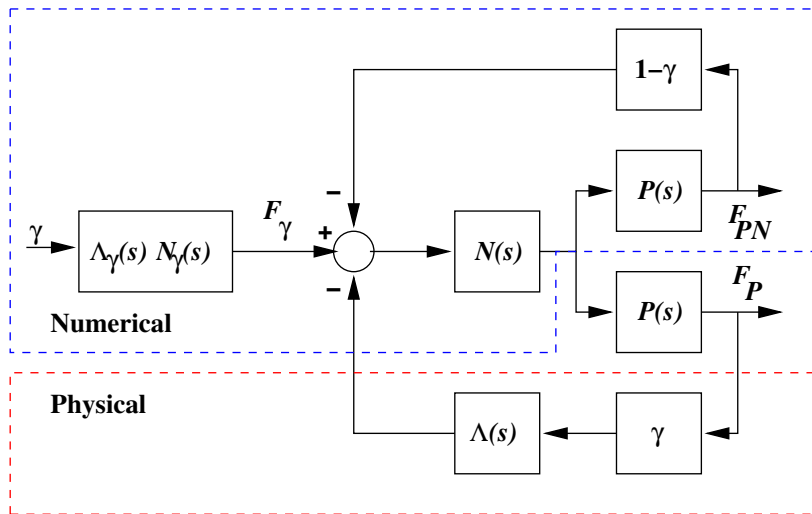


(a) Robustness

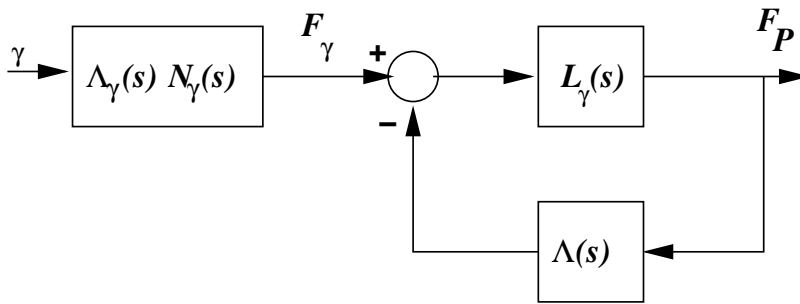


(b) Stability for any delay

Figure 6. Robustness. (a) Shows the inverse magnitude of $D(j\hat{\omega})$ against $j\hat{\omega}$ on a logarithmic scale. For comparison two possible uncertainty transfer functions $e^{-j\hat{\omega}\hat{\tau}}$ and $\frac{1}{1+j\hat{\omega}\hat{\tau}}$ are plotted for $\hat{\tau} = 0.21$. (b) Shows the boundary of stability for *any* delay.

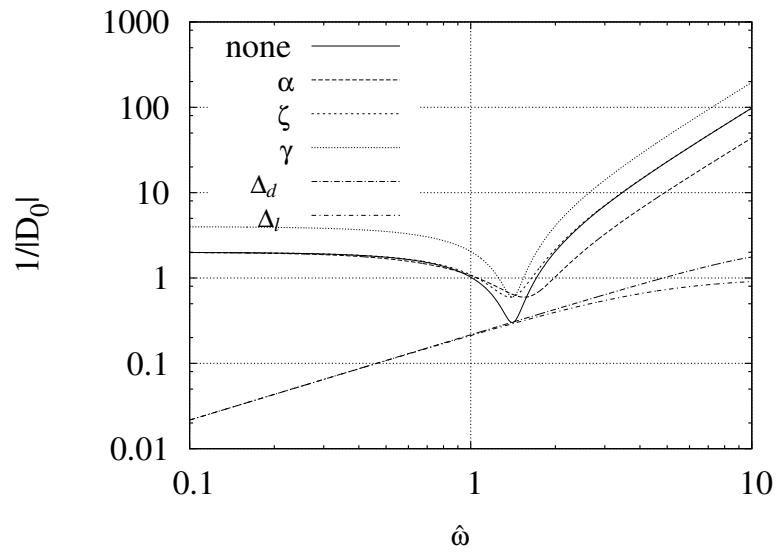


(a) Block diagram

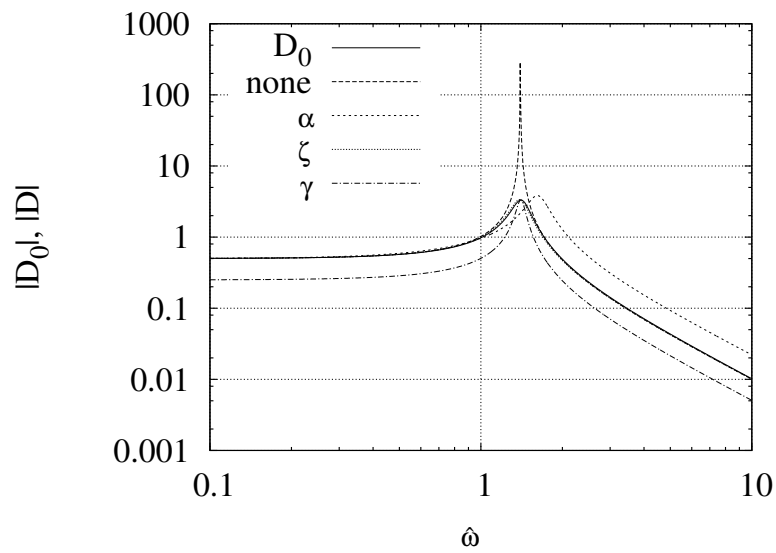


(b) Robustness block diagram

Figure 7. γ -robustness



(a) Robustness analysis



(b) Closed-loop response

Figure 8. Robustness Compensation. (a) The inverse magnitude of $D(j\hat{\omega})$ is plotted against $j\hat{\omega}$ on a logarithmic scale for the three robustness compensators with $\alpha = 1.5$, $\zeta_r = 2\zeta$ and $\gamma = 0.5$. For comparison two possible uncertainty transfer functions $e^{-j\hat{\omega}\hat{\tau}}$ and $\frac{1}{1+j\hat{\omega}\hat{\tau}}$ are plotted for $\hat{\tau} = 0.35$. (b) The lines marked α , ζ and γ give the corresponding closed-loop systems for each compensator, in the presence of $e^{-j\hat{\omega}\hat{\tau}}$. The case of no compensator, with (none) and without (D_0) delay, is given for comparison

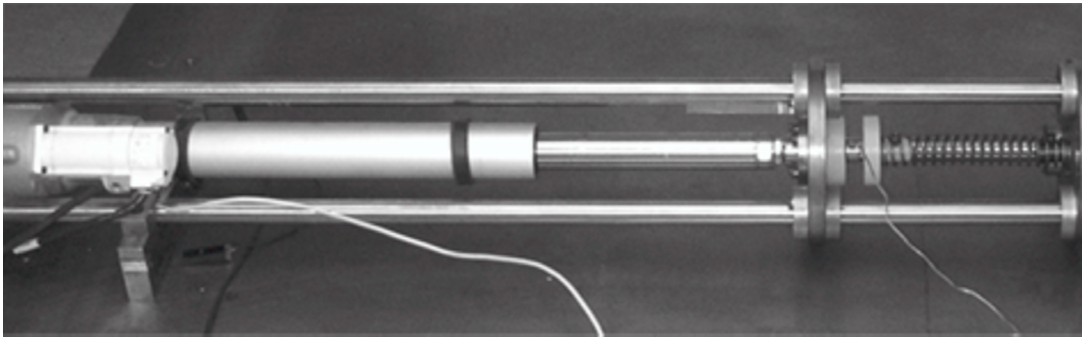


Figure 9. Experimental Equipment: the linear electro-mechanical actuator is on the left of the picture and the physical substructure (spring) is on the right. Two of the three guide rails are visible crossing the picture horizontally.

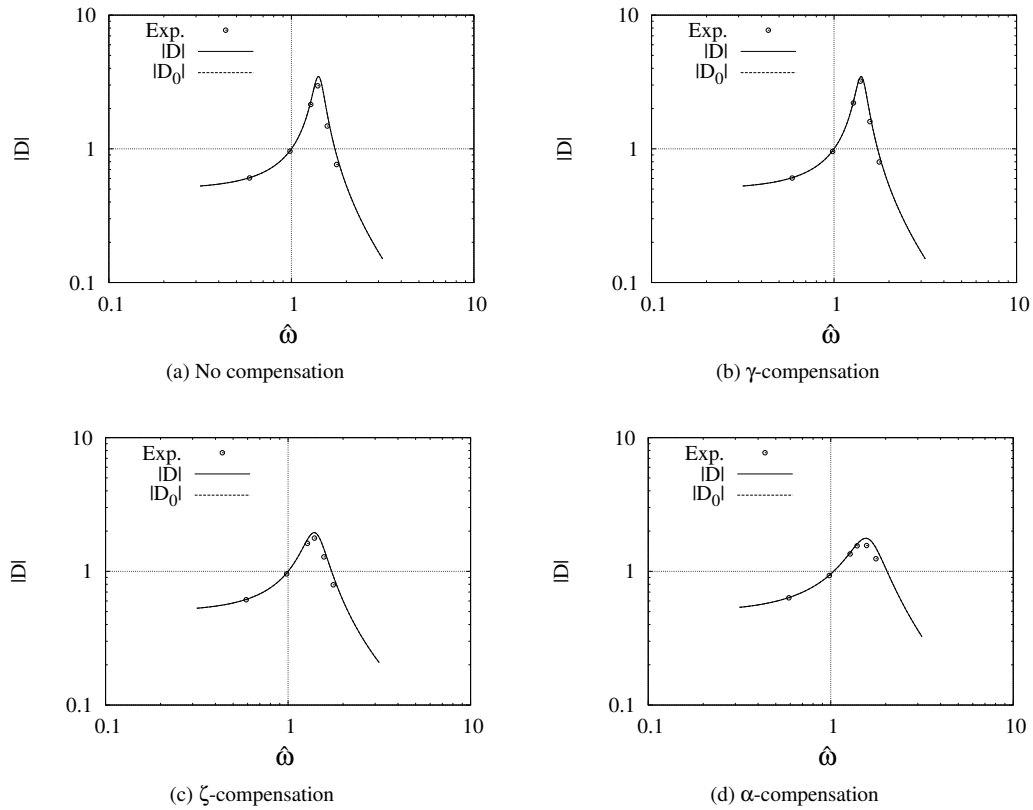


Figure 10. Experimental Results: $\hat{\tau} = 0.00$. In this case the uncertainty is very low so $\Lambda \approx 1$ and $|D| \approx |D_0|$ in all four cases. γ -compensation does not distort $|D|$ but ζ and α -compensation do. The experimental fit is good in each case.

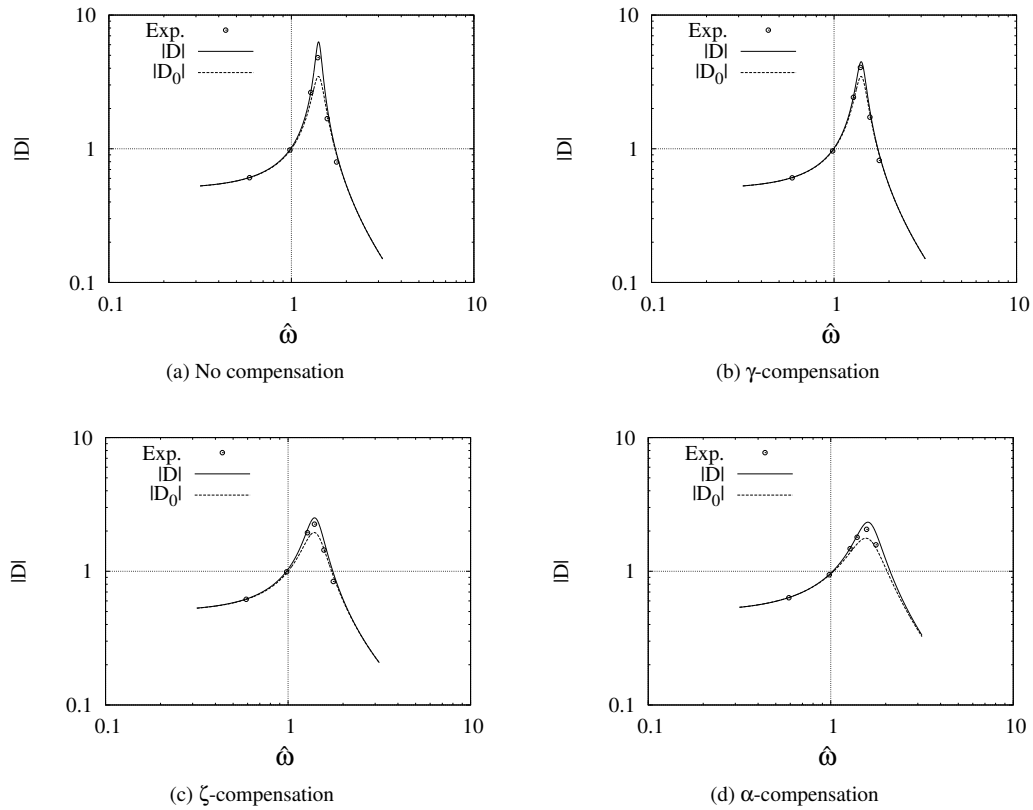


Figure 11. Experimental Results: $\hat{\tau} = 0.10$. There is a small amount of uncertainty due to the neglected delay so $\Lambda \neq 1$ and $|D| \neq |D_0|$ in each case. No compensation leads to an exaggerated resonant peak which is reduced by each of the three compensators. The experimental fit is good in each case.

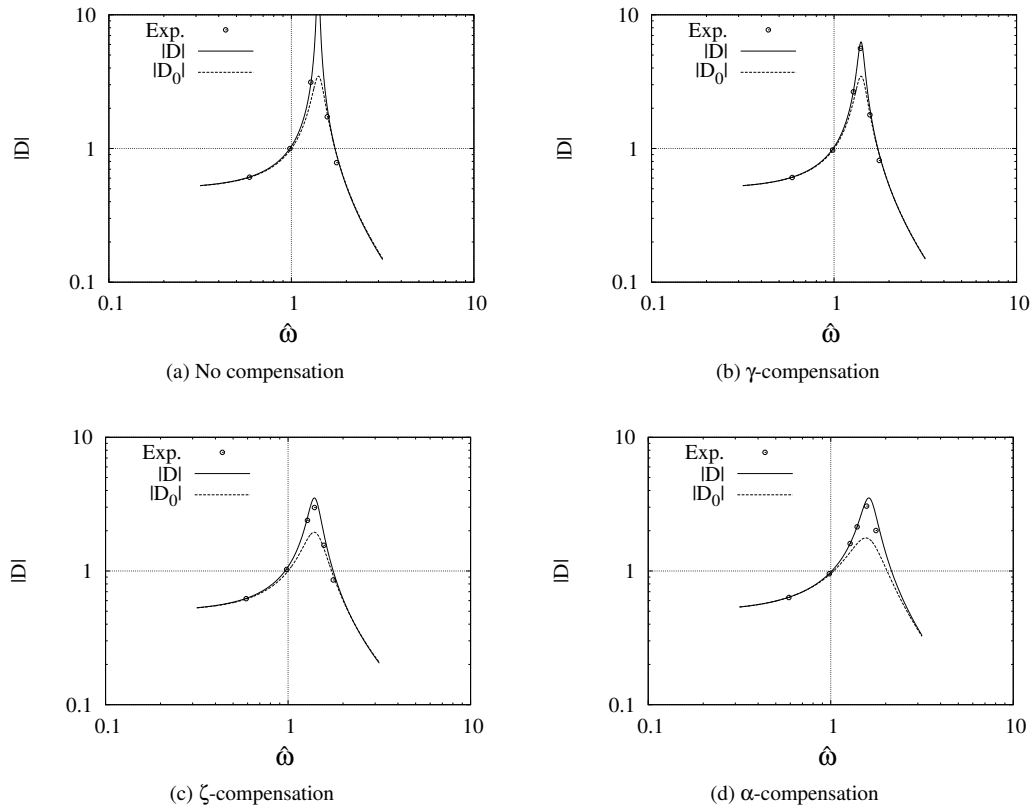


Figure 12. Experimental Results: $\hat{\tau} = 0.19$. There is a large amount of uncertainty due to the neglected delay so $\Lambda \neq 1$ and $|D| \neq |D_0|$ in each case. No compensation leads to an almost unstable system with almost no damping and an excessive resonant peak which far from the nominal. Each of the three compensators stabilises the system giving a peak much closer to the nominal. The experimental fit is good in each case.

List of Tables

I Experiment Summary 36

Fig.	$\hat{\tau}$	$\frac{\hat{\tau}}{\tau_c}$
10	0	0
11	0.1	0.5
12	0.19	0.9

Table I. Experiment Summary